Conference paper

Adem Zengin, Akif Bozkurt, Ismail Hakki Boyaci*, Sadan Özcan, Philippe Daniel, Fabienne Lagarde, Alain Gibaud, Demet Cetin, Zekiye Suludere, Peter Guttmann and Ugur Tamer*

Anisotropic core-shell Fe_3O_4@Au magnetic nanoparticles and the effect of the immunomagnetic separation volume on the capture efficiency

Abstract: The aim of this study was to synthesize in high product yield of anisotropic core-shell Fe_3O_4@Au magnetic nanoparticles and to investigate the effect of the immunomagnetic separation (IMS) volume on the capture efficiency. For these purposes and for the first time, we synthesized polyhedral magnetic nanoparticles composed of Fe_3O_4 core Au shell. To synthesize magnetic gold anisotropic core-shell particles, the seed-mediated synthetic method was carried out. By choosing an appropriate amount of iron particles and growth solution the fine control of the seed-mediated approach is enabled. This led to the high product yield of anisotropic nanoparticles. The magnetic separation of these nanoparticles was easily accomplished, and the resulting nanoparticles were characterized with transmission electron microscopy (TEM), ultraviolet visible spectroscopy (UV–vis), near edge absorption fine structure (NEXAFS) spectroscopy, and X-ray diffraction (XRD). Additionally, the magnetic properties of the nanoparticles were examined. The magnetic nanoparticles (MNPs) were modified with antibody and interacted with *Escherichia coli* (*E. coli*). The high capture efficiency between the magnetic nanoparticles and *E. coli* is evidenced by SEM images. The capture efficiency decreases with an increase of volumes, and the highest capture efficiency was observed for *E. coli* in an experiment volume of 100 μL for magnetic nanoparticles. The percentage of captured *E. coli* for polyhedral nanoparticles was found to be approximately 95 % and for spherical nanoparticles 88 %, respectively.

Keywords: anisotropic nanoparticles; capture efficiency; *Escherichia coli*; immunomagnetic separation; iron-gold magnetic nanoparticles; IUPAC Congress-44, Life Chemistry; scanning electron microscopy (SEM); transmission electron microscopy (TEM).

DOI 10.1515/pac-2013-0915

Article note: A collection of invited papers based on presentations on the Life Chemistry theme at the 44th IUPAC Congress, Istanbul, Turkey, 11–16 August 2013.

***Corresponding authors: Ismail Hakki Boyaci,** Department of Food Engineering, Faculty of Engineering, Hacettepe University, Beytepe 06800 Ankara, Turkey, e-mail: ihb@hacettepe.edu.tr; and **Ugur Tamer,** Department of Analytical Chemistry, Faculty of Pharmacy, Gazi University, Etiler, 06330 Ankara, Turkey, Tel.: +90 312 2023110, Fax: +90 312 2235018, E-mail: utamer@gazi.edu.tr
Adem Zengin: Department of Chemistry, Faculty of Science, Gazi University, 06500 Ankara, Turkey; and Department of Analytical Chemistry, Faculty of Pharmacy, Gazi University, Etiler, 06330 Ankara, Turkey
Akif Bozkurt: Department of Food Engineering, Faculty of Engineering, Hacettepe University, Beytepe 06800 Ankara, Turkey
Sadan Özcan: Department of Engineering Physics, Faculty of Engineering, Hacettepe University, Beytepe 06800 Ankara, Turkey
Philippe Daniel, Fabienne Lagarde and Alain Gibaud: LUNAM Université, Université du Maine, Institut des Molécules et des Matériaux du Mans – IMMM – UMR CNRS 6283, Av. O. Messiaen, 72085 Le Mans Cedex 9, France
Demet Cetin: Science Teaching Programme, Gazi Faculty of Education, Gazi University, 06500 Ankara, Turkey
Zekiye Suludere: Department of Biology, Faculty of Science, Gazi University, 06500 Ankara, Turkey
Peter Guttmann: Helmholtz-Zentrum Berlin für Materialien Energie, Institute of Soft Matter and Functional Materials, Albert-Einstein-Str. 15, 12489 Berlin, Germany

Introduction

The integration of iron oxide nanoparticles and gold or silver shell has been utilized for imaging, magnetic separation, photothermal therapy and targeted drug delivery applications [1–8]. Therefore the synthesis of magnetic nanocomposites would be a crucial step for potential future applications in the next decade [9] like chemical/bio sensors, spectroscopic enhancers and imaging processes. However, the production of monodispersed magnetic nanoparticles remains a big challenge due to the difficulties in synthesizing procedures such as heating, time consumption, as well as the needs for a specific chemical modification to prevent aggregation [10]. In addition, the subject of synthetic strategy is to use lower reaction temperatures [11–17].

One of the examples of the core-shell morphology is to use two-step synthesis strategy [18] involving initial gold layer formation followed by a second shell formation. The similar seed-mediated approaches have shown that anisotropic nanostructures could be generated using gold coated Fe_3O_4 nanoparticles as seeds [19–25]. Various synthetic methods have been also developed for the synthesis of hybrid particles with different shapes [26, 27]. Anisotropic shapes are not thermodynamically favorable due to the formation of low energy facets. However, the addition of capping agents can alter the surface energies for the different crystallographic planes [28]. It was also found that the underpotential deposition (UPD) could account for the anisotropic particle formation when silver ions are added to the reaction mixture [29].

Rapid, selective and sensitive detection methods for bacteria in food, clinical diagnosis and the environment are critical for public health [30, 31]. Conventional identification methods include polymerase chain reaction (PCR) [32], culture and colony counting [33], immunological techniques [34] fluorescence-based enzymatic assays [35] and quantum dots [36]. The advantages of using magnetic nanoparticles for capturing and concentrating bacteria, including the similar size of nanoparticles, magnetic behavior [37] and high capture efficiency are due to high surface-to-volume ratio [38]. Magnetic cell separation is also one of the conventional methods that typically employs the use of antibodies against specific cell surface epitopes to tag cells of interest with magnetic particle conjugates [39]. For a specific interaction to occur, magnetic nanoparticles are usually functionalized with biorecognition molecules, such as antibodies [40], aptamers [41] and carbohydrates [42, 43]. Different factors such as synthesis, shape, size, composition, addition of stabilizers etc. can lead to different conclusions even for the same biological application [44].

In the present work, the seed mediated synthesis method for the preparation of monodisperse anisotropic shaped gold coated iron-oxide nanoparticles in aqueous solution was developed for the first time. The developed synthesis procedure gives the high product yield of anisotropic core-shell Fe_3O_4@Au magnetic nanoparticles. The growth of anisotropic gold coating was achieved after the addition of gold coated Fe_3O_4 particles to a solution of CTAB, $HAuCl_4$, $AgNO_3$ and ascorbic acid at room temperature. The magnetic separation of these nanoparticles was easily accomplished and the resulting nanoparticles were characterized with transmission electron microscopy (TEM), ultraviolet visible spectroscopy (UV–vis), near edge absorption fine structure (NEXAFS) spectroscopy with the HZB-TXM and X-ray diffraction (XRD). The magnetic properties of the nanoparticles were also examined. The effects of shape of the magnetic nanoparticles on immunomagnetic separation (IMS) were also investigated. The effect of the immunomagnetic separation (IMS) volume on the capture efficiency was determined.

Experimental

Chemicals

Biotin-conjugated rabbit anti-*E. coli* polyclonal antibodies were obtained from Fitzgerald Industries International Inc. (Acton, MA, USA). *N*-(3-dimethylaminopropyl)-*N*′-ethylcarbodiimide hydrochloride (EDC), 11-mercaptoundecanoic acid (11-MUA), 2-(*N*-morpholino) ethane sulfonic acid monohydrate (MES), absolute

ethanol, and Tween 20 were obtained from Sigma-Aldrich (Taufkirchen, Germany). Immunopure avidin was obtained from Pierce Biotechnology (Rockford, IL, USA). *N*-Hydroxysulfosuccinimide sodium salt (NHS) was obtained from Pierce Biotechnology (Bonn, Germany). NaCl, Na_2HPO_4, and KH_2PO_4 were from J.T. Baker (Deventer, The Netherlands), used as phosphate-buffered saline (PBS). All solutions were prepared with ultrapure water (18 MΩ cm) to reach the desired concentrations.

Microorganisms

Escherichia coli K12 strain was obtained from Refik Saydam National Type Culture Collections, Ankara, Turkey. The cultures for assay were grown on LB Broth at 37 °C for 18 h. Bacteria samples were prepared by diluting the culture in 0.67 M PBS at pH of 7.4. Also, for *E. coli* detection, LB Agar was used; obtained from Laboratories Conda S.A. (Madrid, Spain) in order to enumerate the number of colony forming units (cfu). For this aim, diluting and plating methods were used and incubation was implemented at 37 °C for 18 h.

Synthesis of spherical core-shell magnetic nanoparticles

The Fe_3O_4 nanoparticles synthesis and Au shell coating procedure were used to fabricate the spherical core-shell magnetic nanoparticles [8].

Synthesis of anisotropic shaped nanoparticles

Magnetic Fe_3O_4 nanoparticles were synthesized by co-precipitation of Fe^{3+} and Fe^{2+} under alkali and inert atmosphere conditions. The precipitate was collected with a magnet and washed twice with excess deionized water and then collected and redispersed in 20 mM trisodium citrate solution and stirred for 24 h to exchange adsorbed hydroxide ions with citrate ions. The citrate stabilized magnetic nanoparticles were precipitated with excess acetone to remove excess citrate anions in the solution. Then, Fe oxide-citrate nanoparticles were dispersed in 10 mL deionized water. For the preparation of core-shell Fe-Au nanoparticles, 500 µL citrate stabilized magnetic nanoparticles were dispersed in 5 mL 0.01 M CTAB solutions. After addition of magnetic nanoparticles, 750 µL 0.01 M Au^{3+} and 250 µL 0.1 M ascorbic acid were added and the solution was stirred for 30 min at room temperature. The gold and ascorbic acid additions were performed two successive times under similar conditions. The obtained spherical Fe-Au core-shell nanoparticles were then collected and washed with deionized water and redispersed in 10 mL of deionized water and used as seed solution.

For the synthesis of the magnetic Fe-Au anisotropic core-shell nanoparticles, 7.5 mL 0.1 M CTAB, 425 µL 0.01 M Au^{3+}, 2.5 µL 0.0478 M Ag^{+}, 750 µL 0.08 M ascorbic acid were sequentially added in 14 mL of deionized water as the growth solution. One milliliter of aforementioned seed solution was added in above solution and stirred gently for 10 s and waited for 24 h without any distribution. The magnetic nanoparticles were collected with a magnet and washed with deionized water and redispersed in deionized water for further characterization.

Preparation of magnetic gold nanoparticle-antibody conjugates, immunomagnetic separation and SEM measurements

The surface of magnetic anisotropic core-shell nanoparticles were modified with the 50 mM 11-MUA in absolute ethanol for overnight to form a self-assembled monolayer (SAM). Nanoparticles were collected using a magnet and washed with ethanol. For surface activation over carboxylate groups, nanoparticles were stirred for 30 min

in NHS/EDC solution. After the activation procedure, the surface was covered with avidin by incubating the nanoparticles in 0.5 mg/mL avidin solution for 40 min to form covalent bonds between avidin and carboxyl groups. The nanoparticles were then interacted with 0.1 mg/mL biotin-labeled antibody in PBS solution to form a biotin-avidin conjugated antibody on the surface. After this procedure, washing was performed with PBS buffer to remove the unconjugated and loosely conjugated biotin-labeled antibodies. In all the washing steps, nanoparticles in washing buffer were placed in an ultrasound bath containing ultrapure water for 10 s.

The effect of the immunomagnetic separation (IMS) volume on the capture efficiency was investigated. For this purpose, the Ab-coated 0.2 mg anisotropic core-shell nanoparticles were mixed with 100 µL *E. coli* (10^3 cfu/mL) in increasing volumes of PBS from 100 µL to 2000 µL and incubated for 30 min at 37 °C on a vortex mixer. The nanoparticles were then separated magnetically and the number of cells (cfu/mL) in each experimental solution was enumerated by plating on LB agar, incubating at 37 °C for 18 h and counting the number of colonies. The non Ab-coated nanoparticles were used as a control of the nanoparticle–bacteria non-specific interactions experiment by following the same procedure as for Ab-coated magnetic nanoparticles. Experiments were performed in duplicates, the average values and standard deviations were calculated. The capturing efficiency is described as the difference between the number of initial bacteria and the number of unbound and loosely bound bacteria divided by the initial number of bacteria multiplied by a hundred. The number of unbound bacteria was determined using plate counting method as described above. It is also given as the formula below, where N_{ib} is number of initial bacteria and N_{ub} is number of unbound bacteria:

$$\text{capturing efficiency} = (N_{ib} - N_{ub}) / N_{ib} \times 100\,\%.$$

For scanning electron microscopic observations, bacterial cells interacted with antibody coated anisotropic magnetic nanoparticles were prepared according to our previous work [45]. Briefly, *E. coli* cells, which had interacted with nanoparticles, were separated from the solution with a magnet and washed three times to remove non specific bindings. Then the sample was placed on a small piece of cover slip. It was fixed overnight in 4 % glutaraldehyde buffered with 0.2 M sodium phosphate (pH 7), and washed three times with 0.2 M sodium phosphate (pH 7) buffer. This was followed by dehydration a graded series of ethanol–water (70, 80, 90, and 100 %). Sample was then added to amyl acetate. The sample was next critical-point dried with CO_2 (Polaron, CPD 7501) and coated with gold (Polaron SC 502 sputter coater).

Instrumentation

Optical absorption spectroscopy measurements were performed in a Spectronics, Genesis model single beam spectrophotometer using 1 cm path length quartz cuvettes. Spectra were collected within a range of 300–800 nm. Transmission electron microscopy (TEM) samples were prepared by pipetting 10 µL of nanoparticle solution onto Formvar–Carbon coated cupper grids and allowed to stand for 10 min. TEM measurements were performed with the Tecnai G2 F30 instrument at 120 kV. XRD measurements were performed using a Philips PW–1140 model diffractometer (Cu Kα radiation at a wavelength of 1.5406 A). Using a Quantum Design Physical Property Measurement System (PPMS) system with a vibration sample magnetometer module, magnetization measurements were done as a function of magnetic field and temperature. Scanning electron micrographs were taken with JEOL JSM 6060 at 10–25 kV. NEXAFS were performed with the Helmholtz Zentrum Merlin (HZB) transmission X-ray microscope (TXM) installed at the BESSY II electron storage ring. A high resolution zone plate objective with 25 nm outermost zone width was used to acquire the image stacks for the spectra.

Results and discussion

Using a combination of CTAB and ascorbic acid as surfactant layer was found to be critical to the formation of anisotropic nanoparticles [46]. Anisotropic core-shells and rhombic dodecahedra with controlled sizes of 30–75 nm were prepared by adjusting the volume of the seed solution added to the growth solution. We

adopted this approach to synthesize Fe_3O_4@Au core-shell anisotropic shaped nanoparticles. Anisotropic shaped magnetic nanoparticles were prepared by a seeded growth method, starting from core-shell Fe_3O_4@Au nanoparticles. Figure 1 shows representative TEM images of the anisotropic nanoparticles and the shape distributions were obtained by measuring 50 individual particles from TEM images. The percentage of anisotropic particles is about 100 %. The production of anisotropic magnetic nanoparticles with high yield is an important step for potential applications and with appropriate adjustment of gold and ligand concentrations, the thickness of shell could be tailored. The anisotropic nanoparticles appeared as clusters on the TEM images due to the magnetic properties of nanoparticles. This procedure gave highly anisotropic nanoparticles with an average diameter of 20 nm. HRTEM analysis of core-shell nanoparticles indicates an epitaxial growth of gold layer as shown in Fig. 2. The measured spacing of gold in the core-shell nanoparticles is 2.5 Å and close to the bulk gold (JCPDS 04-0784: d = 2.35 Å). HRTEM analysis of anisotropic nanoparticles revealed the growth of gold in line with the previous analysis [20].

It is important to note that anisotropic core-shell nanoparticles growth is highly sensitive to the preparation of the growth solution. Recently, Song and co-workers reported that the use of citrate stabilized Fe_3O_4@Au nanoparticles resulted in the growth of star shaped nanostructure, whereas Fe_3O_4@Au nanoparticles dispersed in CTAB solutions promoted isotropic nanostructures [20]. These observations are in agreement with our present study in which CTAB modified gold nanoparticles produced isotropic nanoparticles. Iron oxide

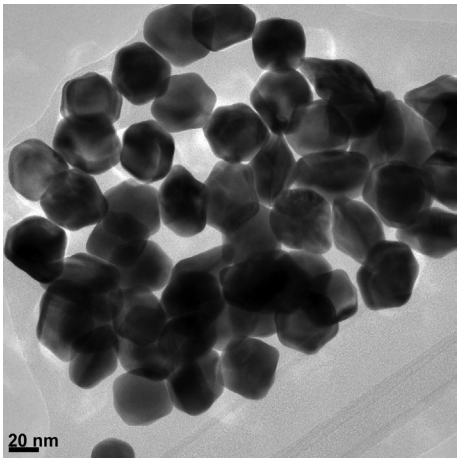

Fig. 1 TEM images of anisotropic core-shell magnetic nanoparticles

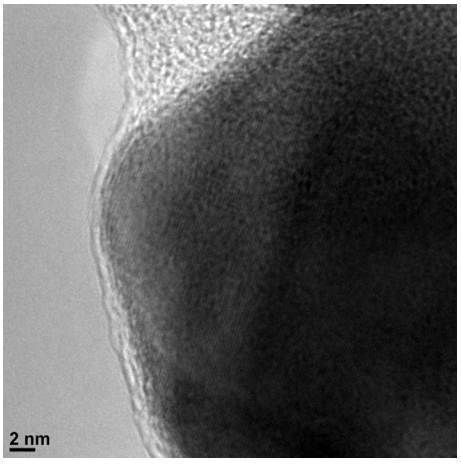

Fig. 2 HRTEM image of core-shell magnetic nanoparticles.

nanoparticle seeds were prepared by basic hydrolysis method [8]. In the present study, core-shell Fe_3O_4@Au nanoparticles were then synthesized from as prepared Fe_3O_4 particles (~ 9 nm) by treatment with $HAuCl_4$ in the presence of CTAB and reducing agent ascorbic acid. The resulting spherical Fe_3O_4@Au core-shell nanoparticles were used as seed solution. The spherical Fe_3O_4@Au nanoparticles are converted into anisotropic shaped Fe_3O_4@Au nanoparticles in the presence of aqueous micellar solutions of CTAB. Gold coating process was carried out in the presence of CTAB to give better particle dispersity and to avoid agglomeration problems. After coating a gold layer onto the iron nanoparticle, zeta potential was found to be +28 mV and agglomeration was not observed due to the presence of CTAB layer onto the magnetic particle surface. All particles have regular polyhedral shapes with narrow size distributions (< 5 %). In comparison with our previous synthesis of anisotropic nanoparticles [27], this seed mediated overgrowth method gave uniform polyhedral shape with a very high yield. However, with respect to the growth solution, we found that in the presence of silver ions, the sequential addition of $HAuCl_4$ to the CTAB solution gave the anisotropic shaped nanostructure. It was already reported that directed surface overgrowth and subsequent shape conversion are not related to the particular shape of the seed, however, anisotropic growth is dependent on the presence of silver ions in the growth solutions [47]. This observation was in agreement with our present results. Addition of the gold ions without silver ions converted the spherical Fe_3O_4@Au to the large size spherical nanoparticles. An obvious transformation from the spherical to anisotropic coating takes place at an Ag/Au molar ratio of 0.028 for this sample. Similar behavior was also observed by Xie research group [48].

Figure 3 shows the extinction spectra of the anisotropic gold-coated iron nanoparticle as well as the spherical gold-coated iron nanoparticle synthesized using the modified seed-mediated growth method. As shown in inset of Fig. 3 suspensions of the resulting nanoparticles generated under optimized growth conditions appeared dark blue color. The observed extinction spectrum shows wide plasmon resonance band around 550 nm of gold layer and the absorbance intensity is decreasing as shown in Fig. 3. On the other hand, spherical gold-coated iron nanoparticles have a plasmon band at 530 nm. The observed red shift is due to the increasing of diameter of the magnetic nanoparticles. It is also considered that magnetic particles tend to aggregate in the solution; eventually anisotropic magnetic nanoparticles show wide peak shape and low absorbance value over the spherical nanoparticles.

The XRD pattern of the anisotropic core-shell magnetic particles is shown in Fig. 4. XRD analysis indicated that the growth of the gold shell match well with that obtained from bulk gold (JCPDS 04-0784; d =

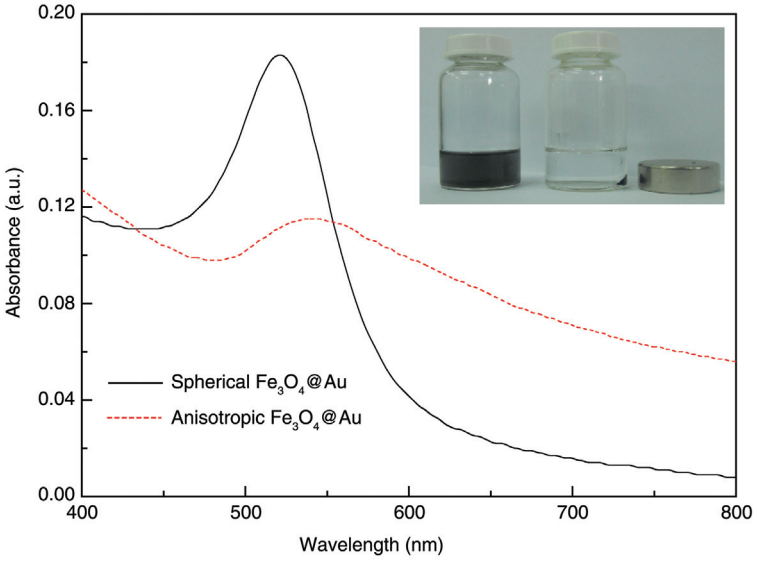

Fig. 3 The extinction spectra of the anisotropic core-shell magnetic nanoparticle and the spherical core-shell magnetic nanoparticles. Inset: The photograph of the anisotropic magnetic nanoparticles taken in the presence of magnetic field and without magnetic field.

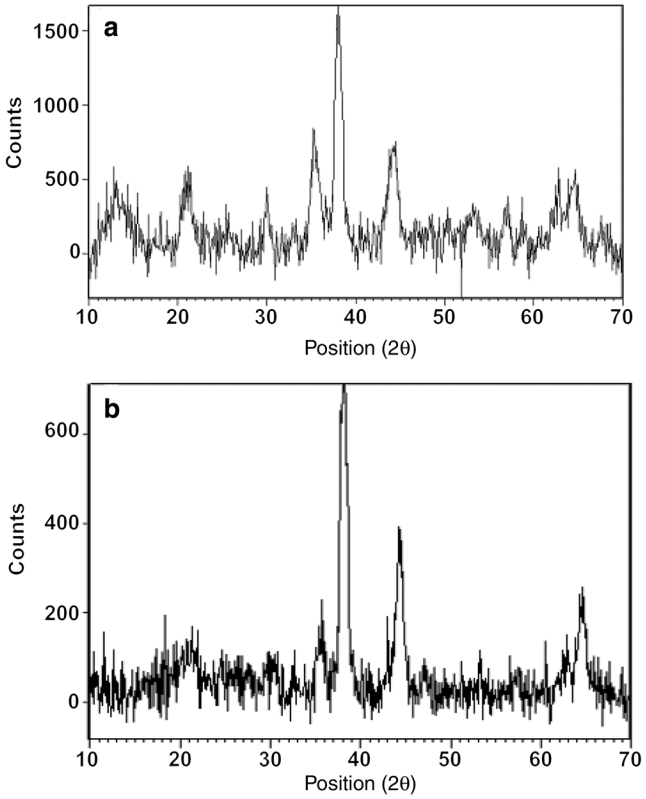

Fig. 4 The XRD pattern of (a) Fe_3O_4 and (b) the anisotropic core-shell Fe_3O_4@Au magnetic nanoparticles.

2.35 Å). All the reflections correspond to gold shell. As labeled in Fig. 3, the peaks at 2θ 38.148, 44.368 and 64.588 are assigned to the Au–Fe position of (111), (200), (220), which are located in the positions of the corresponding materials (JCPDS card No: 04-0784). The crystalline structure of the anisotropic magnetic nanoparticles has proven that the particles are face centered cubic with the dominant crystal planes of 111 and the XRD spectrum shows a 111 diffraction peak of very high intensity relative to the other peaks which indicates the preferred orientation of the 111 faces. The chemical nature of the assemblies was also studied using NEXAFS spectroscopy [49] with the HZB-TXM [50] at the Fe L_3 and L_2 absorption edges. Figure 5 shows the Fe

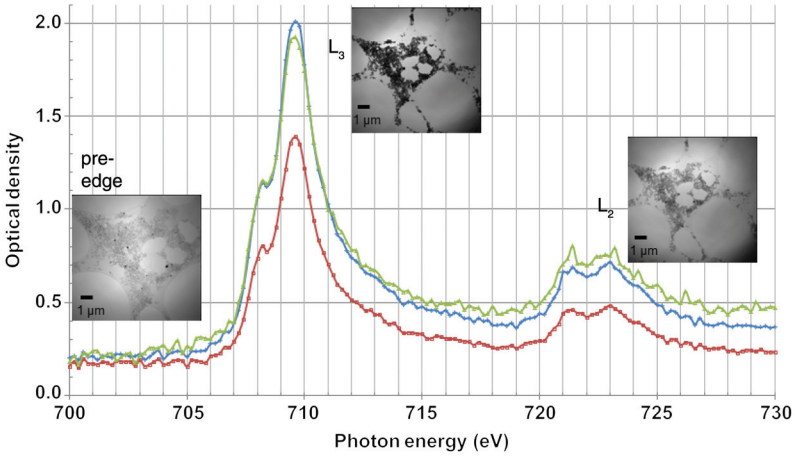

Fig. 5 The Fe L-edge NEXAFS spectra of the magnetic nanoparticles taken at three different sample positions. The insets show X-ray microscopy images taken at different photon energies.

L-edge NEXAFS spectra of the samples taken with three different position for magnetic nanoparticles. The spectra show some oxidation of the iron and the spectrum contains a substantial contribution of the Fe_3O_4 in comparison to the data reported in the literature [51, 52].

The magnetic gold nanoparticles show strong magnetism and the effective separation of nanoparticles was achieved by a simple magnet. The saturation magnetization values for the uncoated and gold coated anisotropic magnetic nanoparticles are shown in Fig. 6. As can be seen, the typical characteristics of superparamagnetic behavior are observed and the saturation magnetization values for the pristine Fe_3O_4 and anisotropic shaped Fe_3O_4@Au nanoparticles were found to be 50 emu/g and 15 emu/g, respectively, at 298 K. The decrease of saturated magnetization was attributed to the formation of the gold layer. Figure 7 shows temperature dependent magnetization (M-T) measurement results for anisotropic magnetic nanoparticles. M-T measurements were performed for sample. In the first part of the experiment, the temperature was lowered to 10 K without applying a magnetic field (zero field cooled, ZFC). At 10 K, a small magnetic field, H = 200 Oe was applied. Then magnetization of the sample was measured as a

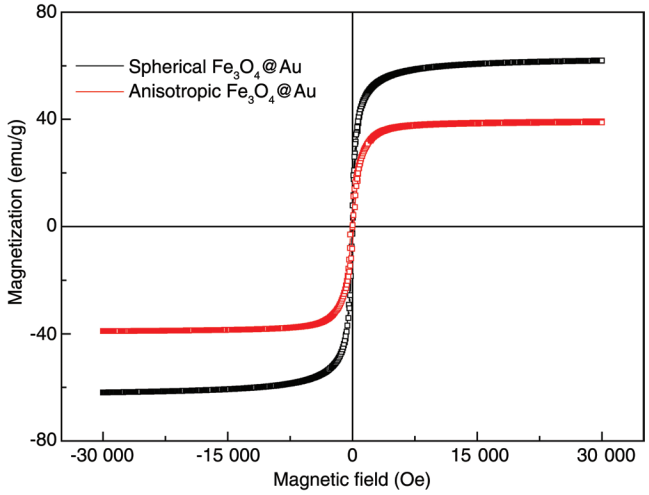

Fig. 6 The saturation magnetization values for the gold coated anisotropic and the spherical magnetic nanoparticles.

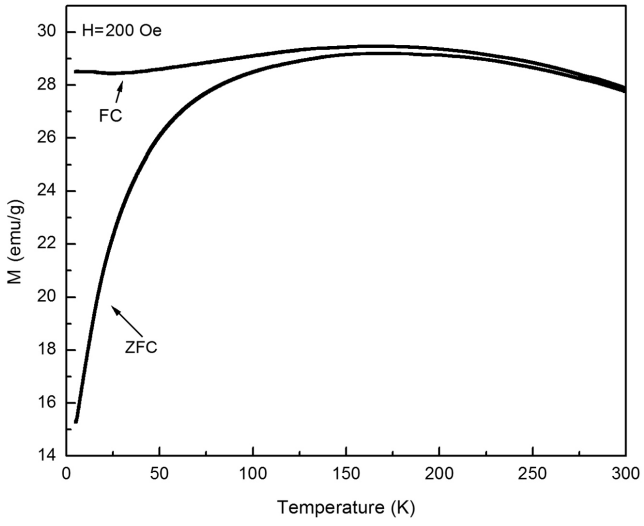

Fig. 7 Zero field cooled (ZFC) and field cooled (FC) curves of the anisotropic magnetic nanoparticles under an applied field of 200 Oe.

function of increasing temperature. When the system reached to 300 K, sample temperature was lowered to $T = 10$ K in the presence of 200 Oe (field cooled, FC). Again magnetization of the sample was measured as a function of increasing temperature. A maximum at 175 K, which is called blocking temperature (T_B) is observed at ZFC measurements of the sample. This result indicated that the sample was superparamagnetic above T_B. The upturn occurring at the low temperature region of FC curve is an indication of particle-particle interactions.

The capture efficiency of IMS

The use of magnetic nanoparticles to separate the bacteria from their matrix was found to be more effective than using the magnetic beads due to the high surface/volume ratio [40]. This approach provided a higher contact surface area resulting in higher capture efficiency. Our previous work [8] also showed that the magnetic nanoparticle based immunoassay system showed similar capture efficiency as compared to the conventional Dynabeads based immunomagnetic separation. We propose that synthesized core-shell anisotropic magnetic nanoparticles can exhibit rapid capture of bacteria from lower separation volumes and bacterial concentrations. For this purpose, the effect of shape of the magnetic nanoparticles on IMS was investigated.

Biofunctionalization of magnetic nanoparticles

Firstly the anisotropic magnetic nanoparticles were modified with 11-mercaptoundecanoic acid then avidin was covalently bounded to the nanoparticle surface via amide linkage. The representative illustration of immuno-magnetic separation procedure is given in Scheme 1. After the EDC/NHS coupling of the magnetic nanoparticles with avidin, zeta potential measurements were carried out and the zeta potentials of the spherical and the anisotropic magnetic nanoparticles were found to be –16.7 and –18.2 mV, respectively. After avidin modifications on the particles surfaces zeta potential values for the spherical and the anisotropic nanoparti-

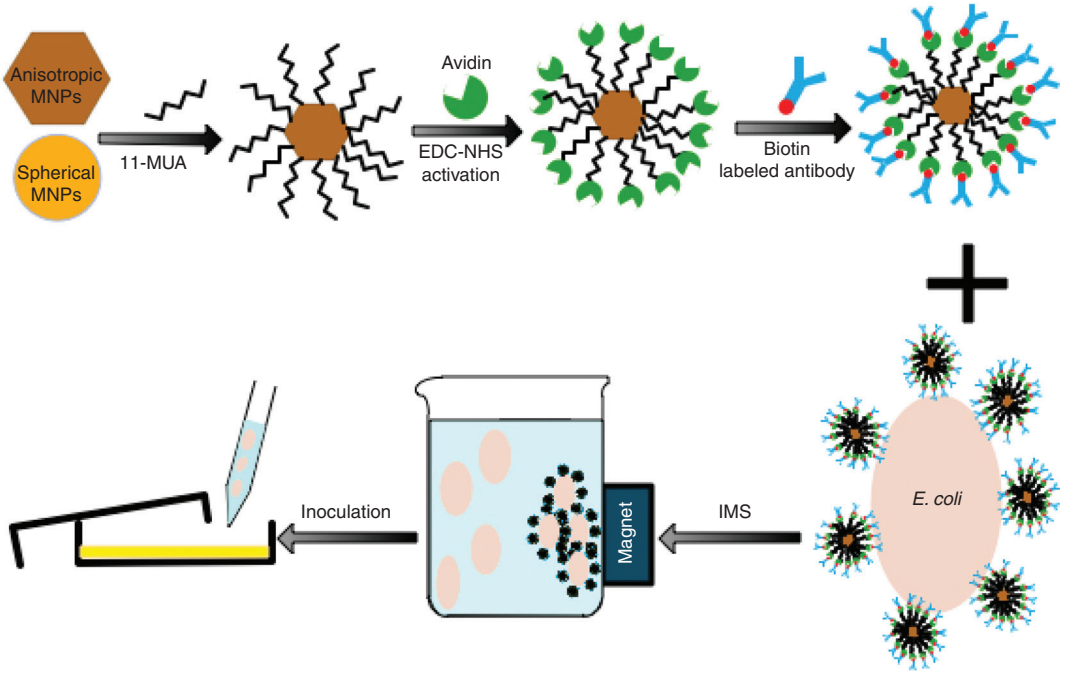

Scheme 1 Representative illustration of immuno-magnetic separation.

cles were found to be –1.39 and 20.3 mV, respectively. The positive shift in zeta potential could be due to the immobilization of avidin on the nanoparticle surface.

To confirm and validate the interaction of antibody modified anisotropic magnetic nanoparticle and *E. coli,* SEM measurements were carried out. The high capture efficiency between magnetic nanoparticle and *E. coli* is also observed by SEM images. It is worth to note that after interactions several washing procedure was made before taking the SEM images to prevent the non-specific binding. As shown in Fig. 8, it is likely that *E. coli* interacts with the antibody on the surface of nanoparticles due to the specific interactions between the bacterial membrane and antibody of magnetic nanoparticles. It is clear that particle aggregation was also observed due to the high magnetic properties of nanoparticles.

The effect of the immunomagnetic separation (IMS) volume on the capture efficiency was investigated. The capture efficiency was found to decrease with an increase of volumes as shown in Fig. 9. The highest capture efficiency was observed for *E. coli* in an experiment volume of 100 µL for both magnetic nanoparticles. The percentage of captured *E. coli* for anisotropic nanoparticles and spherical nanoparticles were found to be approximately 95 and 88 %, respectively. For this reason reactor vessels with a larger number of magnetic particles increase the capture efficiency. High surface area of the nanoparticles gives an opportunity to minimize steric hindrance problem, thus increasing the maximum number of magnetic particles binding to bacteria cell. This work tends to indicate that high capture efficiency in greater volumes of magnetic cell separation depends on optimizing amount of particle and cell number, size and functional abilities of immunomagnetic label such as antibody amplification and blocking particle surfaces for the non-specific interactions.

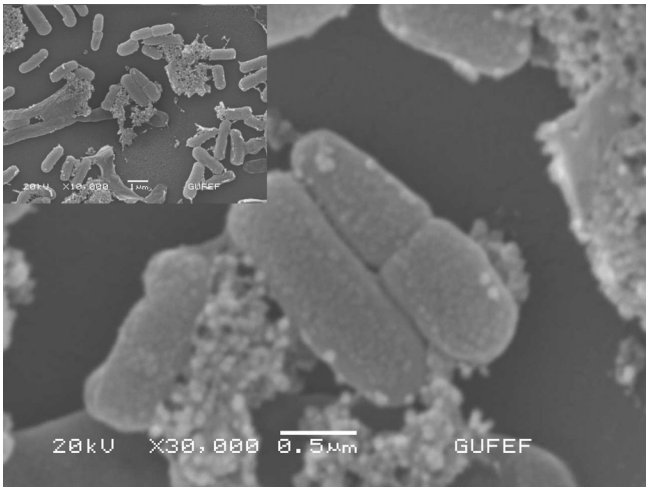

Fig. 8 SEM images of captured bacteria with antibody coated anisotropic magnetic nanoparticles.

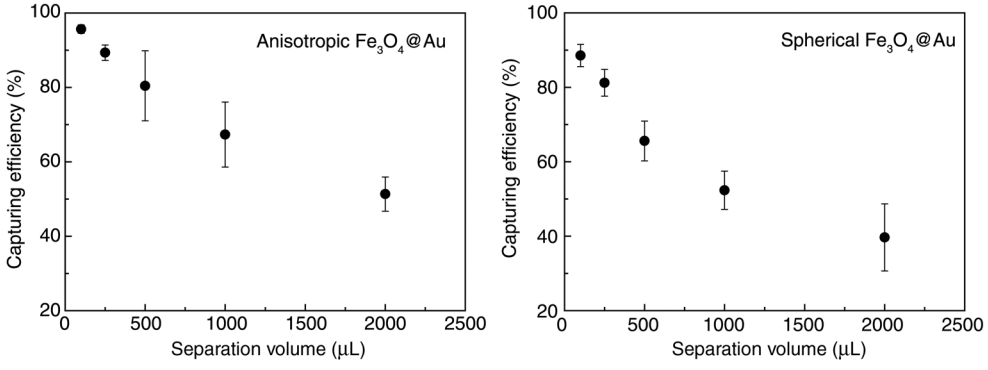

Fig. 9 The capture efficiency of anisotropic and spherical magnetic nanoparticles with increasing volumes.

Conclusions

In the seed mediated synthesis procedure, seed nanoparticles were first produced and several additives can be added to promote the anisotropic growth [20]. As a matter of fact that anisotropic growth is substantially sensitive to the preparation of the growth solution. In this study, anisotropic core-shell nanoparticles were synthesized by dispersing Fe_3O_4@Au nanoparticles in sodium citrate followed by their addition into a growth solution composed of CTAB, $HAuCl_4$, $AgNO_3$ and ascorbic acid acid at room temperature. Choosing appropriate amounts of iron particles and growth solution enabled the fine control of the seed-mediated approach leading to a high product yield of anisotropic nanoparticles. High surface area of the nanoparticles gives an opportunity to bind the maximum number of magnetic particles to the bacteria cell and anisotropic nanoparticles consist of flat surfaces in the form of crystallographic facets and interactions of surface bound ligand are more favorable than the spherical nanoparticles. It was observed that the amount of the magnetic gold nanoparticles played an important role in the analytical procedure to detect *E. coli* in high volumes. These results are then very promising for future applications like new types of biosensors or for bacteria concentrating purposes.

Acknowledgments: In part this work was financially supported by the Helmholtz-Zentrum Berlin (HZB). We gratefully acknowledge the support by the COST action MP0901 "NanoTP" and thank the HZB for allocation of synchrotron radiation beamtime and Gazi University, Faculty of Science for using SEM and TEM facilities. The authors are grateful for the financial support provided by Gazi University research fund and Gazi Bap 05/2011-69.

References

[1] J. S. Aaron, J. Oh, T. A. Larson, S. Kumar, T. E. Milner, K. V. Sokolov. *Opt. Express* **14**, 12930 (2006).
[2] A. L. Timothy, B. James, A. Jesse, S. Konstantin. *Nanotechnology* **18**, 325101 (2007).
[3] J. Schotter, O. Bethge, T. Maier, H. Brueckl. *Appl. Phys. Lett.* **93**, 144105 (2008).
[4] L. Wang, H.-Y. Park, S. I. I. Lim, M. J. Schadt, D. Mott, J. Luo, X. Wang, C. -J. Zhong. *J. Mater. Chem*. **18**, 2629 (2008).
[5] J.-H. Lee, M. A. Mahmoud, V. Sitterle, J. Sitterle, J. C. Meredith. *J. Am. Chem. Soc*. **131**, 5048 (2009).
[6] F. Mohammad, G. Balaji, A. Weber, R. M. Uppu, C. S. S. R. Kumar. *J. Phys. Chem C*. **114**, 19194 (2010).
[7] C. Xu, B. Wang, S. Sun. *J. Am. Chem. Soc*. **131**, 4216 (2009).
[8] U. Tamer, Y. Gündoğdu, İ. H. Boyacı, K. Pekmez. *J. Nanopart. Res*. **12**, 1187 (2010).
[9] C. A. Mirkin, R. L. Letsinger, R. C. Mucic, J. J. Storhoff. *Nature* **382**, 607 (1996).
[10] A. K. Gupta, M. Gupta. *Biomaterials* **26**, 3995 (2005).
[11] M. R. Jones, K. D. Osberg, R. J. Macfarlane, M. R. Langille, C. A. Mirkin. *Chem. Rev*. **111**, 3736 (2011).
[12] J. L. Lyon, D. A. Fleming, M. B. Stone, P. Schiffer, M. E. Williams. *Nano. Lett*. **4**, 719 (2004).
[13] E. E. Carpenter. *J. Magn. Magn. Mater*. **225**, 17 (2001).
[14] E. E. Carpenter, A. Kumbhar, J. A. Wiemann, H. Srikanth, J. Wiggins, W. Zhou, C. J. O'Connor. *Mater. Sci. Eng. C* **286**, 81 (2000).
[15] J. Lin, W. Zhou, A. Kumbhar, J. Wiemann, J. Fang, E. E. Carpenter, C. J. O'Connor. *J. Solid State Chem*. **159**, 26 (2001).
[16] W. L. Zhou, E. E. Carpenter, J. Lin, A. Kumbhar, J. Sims, C. J. O'Connor. *Eur. Phys. J. D* **16**, 289 (2001).
[17] J. Jeong, T. H. Ha, B. H. Chung. *Anal. Chim. Acta* **569**, 203 (2006).
[18] Z. Xu, Y. Hou, S. Sun. *J. Am. Chem. Soc*. **129**, 8698 (2007).
[19] Q. Wei, H.-M. Song, A. P. Leonov, J. A. Hale, D. Oh, Q. K. Ong, K. Ritchie, A. Wei. *J. Am. Chem. Soc*. **131**, 9728 (2009).
[20] H.-M. Song, Q. Wei, Q. K. Ong, A. Wei. *P. ACS Nano* **4**, 5163 (2010).
[21] L. Wang, J. Luo, M. M. Maye, Q. Fan, Q. Rendeng, M. H. Engelhard, C. Wang, Y. Lin, C.-J. Zhong. *J. Mater. Chem*. **15**, 1821 (2005).
[22] L. Wang, J. Luo, Q. Fan, M. Suzuki, I. S. Suzuki, M. H. Engelhard, Y. Lin, N. Kim, J. Q. Wang, C.-J. Zhong. *J. Phys. Chem. B* **109**, 21593 (2005).
[23] C. K. Lo, D. Xiao, M. M. F. Choi. *J. Mater. Chem*. **17**, 2418 (2007).
[24] M. Mandal, S. Kundu, S. K. Ghosh, S. Panigrahi, T. K. Sau, S. M. Yusuf, T. Pal. *M. J. Colloid Interface Sci*. **286**, 187 (2005).
[25] H.-Y. Park, M. J. Schadt, L. Wang, I. I. S. Lim, P. N. Njoki, S. H. Kim, M.-Y. Jang, J. Luo, C.-J. Zhong. *Langmuir* **23**, 9050 (2007).
[26] A. T. Heitsch, D. K. Smith, R. N. Patel, D. Ress, B. A. Korgel. *J. Solid State Chem*. **181**, 1590 (2008).

[27] U. Tamer, İ. Boyacı, E. Temur, A. Zengin, İ. Dincer, Y. Elerman. *J. Nanopart. Res*. **13**, 3167 (2011).
[28] E. Carbó-Argibay, B. Rodríguez-González, J. Pacifico, I. Pastoriza-Santos, J. Pérez-Juste, L. M. Liz-Marzán. *Angew. Chem., Int. Ed*. **46**, 8983 (2007).
[29] M. Liu, P. Guyot-Sionnest. *J. Phys. Chem. B* **109**, 22192 (2005).
[30] C. Kaittanis, S. A. Naser, J. M. Perez. *Nano Lett*. **7**, 380 (2006).
[31] N. Sanvicens, C. Pastells, N. Pascual, M. P. Marco. *TrAC, Trends Anal. Chem*. **28**, 1243 (2009).
[32] L. T. T. Le, C. Cao, J. Hogberg, A. Wolff, D. D. Bang. *Food Control* **24**, 23 (2012).
[33] B. Jarvis, A. J. Hedges, J. E. L. Corry. *Int. J. Food Microbiol*. **116**, 44 (2007).
[34] G. Steve. *Clin. Chem. Lab. Med*. **42**, 1288 (2004).
[35] A. Baumstummler, R. Chollet, H. Meder, F. Olivieri, S. Rouillon, G. Waiche, S. Ribault. *J. Appl. Microbiol*. **110**, 69–79 (2011).
[36] F. C. Dudak, İ. H. Boyaci. *J. Rapid Meth. Aut. Mic*. **16**, 122 (2008).
[37] Y.-F. Huang, Y.-F. Wang, X.-P. Yan. *Environ. Sci. Technol*. **44**, 7908 (2010).
[38] H. Yang, L. Qu, A. N. Wimbrow, X. Jiang, Y. Sun. *Int. J. Food Microbiol*. **118**, 132 (2007).
[39] K. E. McCloskey, J. J. Chalmers, M. Zborowski. *Anal. Chem*. **75**, 6868 (2003).
[40] S. P. Ravindranath, L. J. Mauer, C. Deb-Roy, J. Irudayaraj. *Anal. Chem*. **81**, 2840 (2009).
[41] G. H. Liang, S. Y. Cai, P. Zhang, Y. Y. Peng, H. Chen, S. Zhang, J. L. Kong. *Anal. Chim. Acta* **689**, 243 (2011).
[42] M. J. Anderson, E. Torres-Chavolla, B. A. Castro, E. C. Alocilja. *J. Nanopart. Res*. **13**, 2843 (2011).
[43] E. Valero, S. Tambalo, P. Marzola, M. Ortega-Muñoz, F. J. López-Jaramillo, F. Santoyo-González, J. de Dios López, J. J. Delgado, J. J. Calvino, R. Cuesta, J. M. Domínguez-Vera, N. Gálvez. *J. Am. Chem. Soc*. **133**, 4889 (2011).
[44] S. Chatterjee, A. Bandyopadhyay, K. Sarkar. *J. Nanobiotechnol*. **9**, 34 (2011).
[45] U. Tamer, D. Cetin, Z. Suludere, I. H. Boyaci, H. T. Temiz, H. Yegenoglu, P. Daniel, İ. Dinçer, Y. Elerman. *Int. J. Mol. Sci*. **14**, 6223 (2013).
[46] H.-L. Wu, C.-H. Kuo, M. H. Huang. *Langmuir* **26**, 12307 (2010).
[47] D. Seo, C. I. Yoo, J. C. Park, S. M. Park, S. Ryu, H. Song. *Angew. Chem., Int. Ed.* **47**, 763 (2008).
[48] Y. Xiang, X. Wu, D. Liu, Z. Li, W. Chu, L. Feng, K. Zhang, W. Zhou, S. Xie. *Langmuir* **24**, 3465 (2008).
[49] J. Stöhr. *NEXAFS Spectroscopy*, Springer, Berlin (1992).
[50] P. Guttmann, C. Bittencourt, S. Rehbein, P. Umek, X. Ke, G. Van Tendeloo, G. Schneider. *Nat. Photonics* **6**, 25 (2011).
[51] S. Anders, S. Sun, C. B. Murray, C. T. Rettner, M. E. Best, T. Thomson, M. Albrecht, J. U. Thiele, E. E. Fullerton, B. D. Terris. *Microelectron. Eng*. **61–62**, 569 (2002).
[52] S. Kumar, K. M. Batoo, S. Gautam, B. H. Koo, A. Muddin K. H. Chae, H. Chung, C.G. Lee. *J. Nanosci. Nanotechnol*. **11**, 396 (2011).